

Dynamical phases of the Hindmarsh-Rose neuronal model: Studies of the transition from bursting to spiking chaos

Giacomo Innocenti^{a)}

Dipartimento di Sistemi ed Informatica, Università di Firenze, via S. Marta 3, 50139 Firenze, Italy and Centro Interdipartimentale per lo Studio di Dinamiche Complesse, Università di Firenze, I-50019 Sesto Fiorentino, Italy

Alice Morelli

Dipartimento di Sistemi ed Informatica, Università di Firenze, via S. Marta 3, 50139 Firenze, Italy, Istituto Nazionale di Ottica Applicata, Consiglio Nazionale delle Ricerche, Largo E. Fermi, 5, I-50125 Firenze, Italy, and Centro Interdipartimentale per lo Studio di Dinamiche Complesse, Università di Firenze, I-50019 Sesto Fiorentino, Italy

Roberto Genesio

Dipartimento di Sistemi ed Informatica, Università di Firenze, via S. Marta 3, 50139 Firenze, Italy and Centro Interdipartimentale per lo Studio di Dinamiche Complesse, Università di Firenze, I-50019 Sesto Fiorentino, Italy

Alessandro Torcini^{b)}

Istituto dei Sistemi Complessi, Consiglio Nazionale delle Ricerche, via Madonna del Piano, 10, I-50019 Sesto Fiorentino, Italy, Istituto di Fisica Nucleare, Sezione di Firenze, I-50019 Sesto Fiorentino, Italy, and Centro Interdipartimentale per lo Studio di Dinamiche Complesse, Università di Firenze, I-50019 Sesto Fiorentino, Italy

(Received 31 August 2007; accepted 5 November 2007; published online 28 December 2007)

The dynamical phases of the Hindmarsh-Rose neuronal model are analyzed in detail by varying the external current I . For increasing current values, the model exhibits a peculiar cascade of nonchaotic and chaotic period-adding bifurcations leading the system from the silent regime to a chaotic state dominated by bursting events. At higher I -values, this phase is substituted by a regime of continuous chaotic spiking and finally via an inverse period doubling cascade the system returns to silence. The analysis is focused on the transition between the two chaotic phases displayed by the model: one dominated by spiking dynamics and the other by bursts. At the transition an abrupt shrinking of the attractor size associated with a sharp peak in the maximal Lyapunov exponent is observable. However, the transition appears to be continuous and smoothed out over a finite current interval, where bursts and spikes coexist. The beginning of the transition (from the bursting side) is signaled from a structural modification in the interspike interval return map. This change in the map shape is associated with the disappearance of the family of solutions responsible for the onset of the bursting chaos. The successive passage from bursting to spiking chaos is associated with a progressive pruning of unstable long-lasting bursts. © 2007 American Institute of Physics.

[DOI: [10.1063/1.2818153](https://doi.org/10.1063/1.2818153)]

Neuronal membranes display an excitable electrical activity due to the out-of-equilibrium conditions in which they are maintained by virtue of active ionic pumps. Under the action of external stimuli the membrane potential can exhibit complicated dynamical evolution in connection with variations of the intramembrane ionic currents. Signals among neurons are probably transmitted as patterns of action potentials (spikes) of different complexity. The most common signals are constituted by continuous firing of action potentials (i.e., spiking dynamics) or by oscillations between tonic spiking and a silent (resting) state (i.e., bursting dynamics). Phenomenological and neurophysiological models developed to reproduce the electrical activity of cell membranes have provided many

nontrivial examples of dynamical systems. The richness of the behaviors exhibited by these models is often associated with extremely complicated bifurcation diagrams. The Hindmarsh-Rose (HR) model represents a paradigmatic example of these systems, since it is able to reproduce spiking or bursting dynamics upon variation of an external parameter (the dc current). Besides a rich bifurcation diagram, the HR model displays two different chaotic regimes: one dominated by bursts and one by spiking solutions. The characterization of these two dynamical phases and of the transition connecting them is the subject of our analysis.

I. INTRODUCTION

Several models have been introduced to reproduce the bursting behavior of neuronal cells, in particular the development of the Hindmarsh-Rose (HR) model¹ was stimulated

^{a)}Electronic mail: giacomo.innocenti@gmail.com.

^{b)}Electronic mail: alessandro.torcini@isc.cnr.it.

by the studies of bursting neurons of the pond snail *Lymnaea*, while various other theoretical models²⁻⁵ have been triggered by the analysis of the activity of pancreatic β -cells.

The main characteristics of the dynamics of all these models can be summarized as follows: by varying a control parameter (e.g., an external dc current) the system passes from a situation where it exhibits stable bursting solutions to a regime characterized by continuous spiking. Moreover the transition from bursting to spiking is typically chaotic and it has been analyzed for the HR model in two previous papers.^{6,7} In both these works the transition has been identified as a crisis which destabilizes the chaotic state of continuous spiking, González-Miranda has defined this transition a *continuous interior crisis*,⁷ while Wang suggested that the genesis of the bursting state should be related to the realization of a homoclinic reinjection mechanism to an unstable chaotic saddle born at the crisis.⁶ These two authors provided two different criteria to identify the transition: for González-Miranda this is characterized by a sharp drop in the size of the three-dimensional attractor, or analogously in the spread of the interspike intervals (ISIs); for Wang during the phase of spiking (resp. bursting) the associated attractor is restricted (resp. not restricted) to one side of the invariant manifold associated with the stable and weakly unstable directions of the fixed point of the system.

Another peculiar feature of these models is the occurrence of a *cascade* of period-adding bifurcations leading from the silent regime to repetitive bursting, each bifurcation being characterized by the increase of one unit in the number of spikes forming the burst.⁸⁻¹¹ In 1991 Terman⁸ showed, in a general framework, that this kind of transition could be either continuous or discontinuous. In the first case a stable periodic solution modifies smoothly from n to $n+1$ spikes and during the transition the period of the burst itself becomes extremely long, while in the second case a Smale horseshoe can arise during the transition, but its nature would be essentially repulsive.¹² However, numerical results reported more recently for models of the pancreatic β -cell seem to somehow contradict the scenario depicted by Terman. In particular, in Ref. 10 the authors have shown, by examining the Sherman model,⁵ that stable n -spike bursts cease to exist due to subcritical period doubling bifurcations and stable bursts with $n+1$ -spike emerge in correspondence to saddle-node bifurcations. At the transition there is a coexistence region for stable bursts with n and $n+1$ spikes, whose basin of attractions reveal boundaries with a fractal structure. These differences could be due to the fact that the Terman results are essentially based on an analysis of the fast subsystem (FS), once the system itself has been decomposed in a fast and a slow part. Indeed this approach allows a drastic simplification of the dynamics, but it can lead to misleading conclusions.¹⁰ Moreover, in Ref. 9 the analysis of the Chay neuron model² has revealed that, in absence of chaos, the sequence of period-adding bifurcations for the bursts can be put in direct relationship with the period doubling cascade involving the spiking solutions.

In the present article, we aim at re-examining in the context of the HR model the nonchaotic and chaotic period adding bifurcations²³ as well as the transition from the cha-

otic bursting state to the chaotic spiking phase. The nonchaotic bifurcation sequence is analyzed in details by discussing general aspects of these period adding bifurcations and differences with respect to previous analysis of similar scenarios reported for other bursting neurons. The chaotic period adding bifurcation is characterized in terms of Lyapunov exponents as well as by estimating the distributions of *regular* and *anomalous* bursts. In order to describe the transition from bursting chaos (BC) to spiking chaos (SC), we introduce as an order parameter the maximal number of spikes occurring within a (regular) burst. Moreover, the investigation of the transition is performed by considering the ISI sequences and the associated return maps combined with the Lyapunov analysis and the bursts distributions.

In Sec. II the model will be introduced together with the main dynamical indicators employed here. In order to give a first general description of the possible dynamical behaviors present in the HR model Sec. III will be devoted to an analysis of the phase diagram of the associated FS. The bifurcation diagram of the complete model will be discussed in Sec. IV, with particular emphasis on the period-adding nonchaotic bifurcations. The chaotic bifurcations as well as the transition from BC to SC will be the subject of Sec. V. A short summary of the main results will be reported in Sec. VI.

II. MODEL AND TOOLS

In the present paper we will limit our analysis to the HR model, that can be written in the following way:

$$\begin{aligned} \dot{x} &= 3x^2 - x^3 + y - z + I, & \dot{y} &= 1 - 5x^2 - y, \\ \dot{z} &= r \left[4 \left(x + \frac{8}{5} \right) - z \right]. \end{aligned} \quad (1)$$

We will examine the dynamics of the model for two values of the parameter r (namely, $r=0.0021$ and 0.001) by varying the external dc current I . The model has been integrated by employing Runge-Kutta schemes, usually a fourth order with time step $\Delta t=0.0002-0.0001$, but in some cases also a variable time step fourth to fifth order algorithm with absolute precision of $10^{-6}-10^{-7}$ has been used.

In order to study the bifurcation diagram of Eq. (1) we will employ the continuation software AUTO 2000,¹³ while the linear stability of the solutions is analyzed in terms of their Floquet eigenvalues. The degree of chaoticity of the whole dynamics is measured in terms of the Lyapunov spectrum $\{\lambda_k\}(k=1,2,3)$, evaluated by integrating the linearized dynamics associated with Eq. (1) and by performing periodic Gram-Schmidt ortho-normalizations according to the method reported in Ref. 14. The Lyapunov exponents λ_k are real numbers ordered from the largest to the smallest, a positive maximal Lyapunov λ_1 indicates that the dynamics of the system is chaotic. Moreover, from the knowledge of the Lyapunov spectrum it is possible to obtain an estimation of the number of degrees of freedom actively involved in the chaotic dynamics in terms of the Kaplan-Yorke dimension¹⁵ $d_{KY}=j+\sum_{k=1}^j \lambda_k/|\lambda_{j+1}|$, j being the maximal index for which $\sum_{k=1}^j \lambda_k \geq 0$.

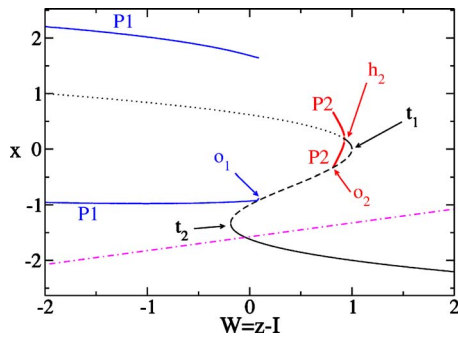


FIG. 1. (Color online) Extrema of x for the stationary solutions of the FS (2) vs the parameter W . The S-shaped line refers to the FPs, while the extrema of the periodic solutions P1 (resp. P2) are shown in blue (resp. red). Solid (resp. dotted) lines indicate stable (resp. unstable) solutions, while the dashed ones are associated with saddles. The dot-dashed straight line is the z -nullcline (3) for $I=0.10$. In particular, $h_1 \equiv (W(h_1), x(h_1)) = (-11.5932, 1.8164)$, $h_2 = (0.9264, 0.1835)$, $t_1 = (1.0000, 0.0000)$, $t_2 = (-0.1851, -1.3333)$, $o_1 = (0.0856, -0.9194)$, and $o_2 = (0.8162, -0.3317)$.

As previously shown in Refs. 6 and 16 and due to the fact that one direction is strongly contracting, the dynamics of the present model can be well described in terms of a one-dimensional map of the interval. Typically a Poincaré section has been employed to construct such a map, instead we will analyze the first return map associated with the sequence of ISIs, similarly to what was recently done in Ref. 17. Since the time series associated with the ISIs usually contains sufficient information to reconstruct the dynamics of a spiking system.¹⁸

III. THE FAST SUBSYSTEM

The HR model has been devised to reproduce bursting behavior of neurons and it has been developed from a simpler two-dimensional model exhibiting an S-shaped stability curve for the corresponding fixed point (FP) coexisting with stable periodic solutions (i.e., with regular spiking). The third added variable has a slower dynamics (whose time scale is ruled by the parameter r) and for specific values of the current the presence of this third variable allows the system to pass from the silent regime to the repetitive firing behavior during a periodic cycle, thus giving rise to bursts of different complexity.

Due to the smallness of the r parameter the time dynamics of the system can be decomposed in a slow and a fast evolution. Moreover, the analysis of the FS can already lead to a reasonable comprehension of the behavior of the whole model.^{8,19} The equations for the FS can be rewritten as

$$\dot{x} = 3x^2 - x^3 + y - W, \quad \dot{y} = 1 - 5x^2 - y, \quad (2)$$

where $W = z - I$ plays the role of an external parameter. These equations admit FP solutions coexisting with stable periodic ones, that are displayed in Fig. 1. The FP solutions exhibits the typical S-shaped form, in particular in the lower branch the FP is stable, while in the intermediate branch becomes a saddle [for $W(t_2) < W < W(t_1)$, see Fig. 1]. In the upper branch the situation is more complicated, at very large negative W -values (not displayed in Fig. 1) the FP is stable, then it loses its stability via a supercritical Hopf bifurcations at h_1

where a first family of periodic stable solutions (P1) emerges surrounding the unstable FP. The family P1 disappears when the periodic orbit collides with the FP metastable branch at the homoclinic point o_1 . By following the upper branch towards larger W -values, the FP turns from unstable to stable at h_2 . Another family of stable periodic orbits (P2) coexist with the unstable FP in the interval $W(o_2) < W < W(h_2)$; they emerge via a supercritical Hopf bifurcation at h_2 and disappear at o_2 , due to a homoclinic collision with another saddle. By further following the upper branch for larger W , the stable FP loses its stability via a tangent bifurcation by colliding with a saddle at t_1 . Finally another tangent bifurcation interests the FP at t_2 where the saddle branch and the lower branch of stable solutions collides.

Since we consider quite small r -values the phase diagram associated with the FS reported in Fig. 1 will be extremely useful to help in understanding the dynamics and the bifurcations of the complete 3D model (1). In particular, the family P1 of periodic orbits will be associated with the bursting and spiking dynamics of the complete model, while the family P2 plays a fundamental role in the nonchaotic period-adding bifurcations.

IV. THE BIFURCATION DIAGRAM OF THE COMPLETE SYSTEM

In the present section we will illustrate the sequence of bifurcations observed for the complete model (1) for $r = 0.0021$ by varying the external current I .

A. Fixed point bifurcations

The system always admits a unique FP, that is given by the intersection of the z null cline,

$$x = \frac{z}{4} - \frac{8}{5} = \frac{W + I}{4} - \frac{8}{5} \quad (3)$$

with the curve representing the stationary FPs for the FS reported in Fig. 1. Let us start from very large currents, in this case the FP is located in the upper branch shown in Fig. 1 at very negative W -values as it is stable. It loses its stability at $I=25.2612$ (corresponding to h_1 for the FS) via a supercritical Hopf bifurcation that gives rise to a stable limit cycle, that will remain stable until $I=3.2195$. We will later investigate the bifurcations of the periodic solutions. For the moment, let us limit the analysis to the FP stability. The FP returns stable at $I=6.1976$ (corresponding to h_2 for the FS) where a subcritical Hopf bifurcation takes place. Therefore for $I \leq 6.1976$ we have the coexistence of a stable FP with two limit cycles, one stable and one unstable. At $I=5.3978$ (corresponding to t_1 in Fig. 1) the FP will again lose its stability via a supercritical Hopf bifurcation and we have the coexistence of two stable limit cycles. The FP will remain unstable for a large current interval (the most relevant one for the complex dynamics of the model) up to $I=1.2895$ (corresponding to t_2 in Fig. 1) where it will become definitively stable via a subcritical Hopf bifurcation.

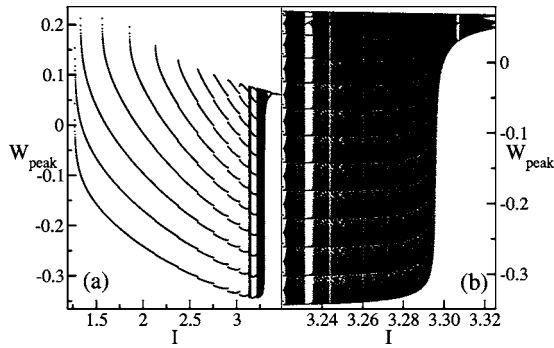


FIG. 2. Peak positions $W_{\text{peak}} = z_{\text{peak}} - I$ as a function of the current I . The whole bifurcation diagram is shown in (a), while in (b) a magnification of the chaotic region is reported. The data refers to $r=0.0021$ and they have been taken after discarding a transient period $T \sim 10^5$.

B. Spiking solutions: Period doubling cascade

As already mentioned, a stable limit cycle emerges at $I = 25.2612$ and it has a pure sinusoidal shape, by decreasing the current value the shape modifies and the periodic solution becomes a train of identical spikes. This solution gives rise to a cycle characterized by two spikes per period at $I = 3.3703$ via a period doubling bifurcation. Finally, a cascade of period doubling leads the system to a chaotic (spiking) state at a current $I_{cs} = 3.3242(1)$. The cascade is shown in Fig. 2 by reporting the peak positions $W_{\text{peak}} = z_{\text{peak}} - I$ vs I . The nonchaotic regular spike trains, composed by one or more spikes per cycle, corresponds to the family P1 of periodic solutions found in the FS. A typical spiking solutions is shown in Fig. 3(a).

C. Bursting solutions: Period-adding bifurcations

In this subsection we discuss how the bursting solutions will emerge from the stable FP present at low current values by increasing I . The FP is initially the unique solution of the system and it is stable until $I = 1.2895$, where due to a subcritical Hopf bifurcation it becomes unstable [see Fig. 4(a)]. In correspondence of this transition point an unstable limit cycle emerges and turns stable via a saddle-node bifurcation occurring at $I = 1.2685$ [SN_{1a} in Fig. 4(a)]. This stable limit cycle is termed “burst” and it is different from the stable spiking solutions described before, since the orbit in this case does not remain always confined in the vicinity of the branch of periodic solutions P1 of the FS, but it spends also a large part of the cycle in proximity of the stable FP of the FS [as shown in Fig. 3(b)]. This solution, characterized by only one spike, disappears via a second saddle-node bifurcations (SN_{1b}) at $I = 1.27018$, while a stable burst with two spikes appears at a lower current $I = 1.27017$ (SN_{2a}) again via a tangent bifurcation. It should be noticed that in the interval $[1.2685; 1.2895]$ the stable FP coexists with stable bursts. By increasing I a peculiar sequence of saddle-node bifurcations can be observed: the burst with k -spikes disappears at SN_{kb} and a new burst with $k+1$ -spikes arises at a lower current via a tangent bifurcation at SN_{k+1a} , moreover the two stable solutions with k and $k+1$ peaks are continuously connected via a branch of unstable bursting solutions [see Fig. 4(b)]. As a final remark, the two stable bursting solutions coexist in a

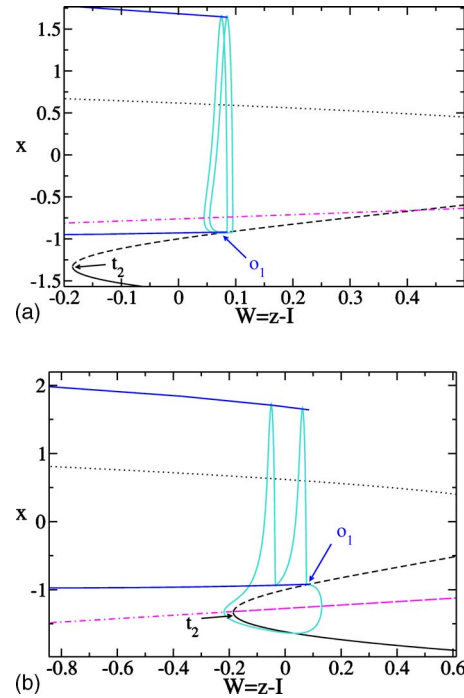


FIG. 3. (Color online) Extrema of x corresponding to the stationary solutions of the FS (2) versus W together with stable solutions of the complete HR model. In (a) a spiking solutions with two spikes per cycle is reported for $I=3.35$; while in (b) a bursting solution with two peaks per burst is shown for $I=1.30$. The symbols are as in Fig. 1 and the dot-dashed (magenta) z null clines refer to the examined currents.

small current interval. This period-adding transition is quite similar to the one described in Ref. 10 apart from the fact that in that paper the authors have identified the first transition (where the k -spike burst ceases to exist) as a subcritical period-doubling.

As we have mentioned the emergence of the new spike in the burst is a continuous process, if one includes in the picture also the unstable solution interpolating between the stable bursts with k and $k+1$ spikes. Since this scenario is common to all the period-adding bifurcations (in absence of chaos) we will limit to analyze the transition from four to five spikes reported in Fig. 4(b). At $I = 1.85457$ the four-spike burst disappears by colliding with an unstable solution. By following the unstable solution for decreasing currents one observes a peculiar increase in the duration of the burst by approaching the SN_{5a} (at $I \equiv I^* = 1.8541367022$), as it can be clearly appreciated in Fig. 5. The period of the solution increases because the orbit once reached the homoclinic point o_1 is not attracted (as expected) by the stable branch, but it instead follows the “metastable” saddle branch towards t_1 [as shown in Fig. 5(a)]. By decreasing I the orbit finally reaches t_1 and then the orbit folds back being attracted by the family P2 of (stable in the FS) periodic solutions. This gives rise to an additional peak in the burst structure and the solutions with one extra peak gets finally stabilized at SN_{5a} . A similar mechanism for the period-adding bifurcation has been suggested by Terman⁸ for a continuous nonchaotic transition. However Terman suggested that the solution should remain stable during the whole transition, but this does not seem to be true for the HR model. Moreover, exactly at SN_{5a}

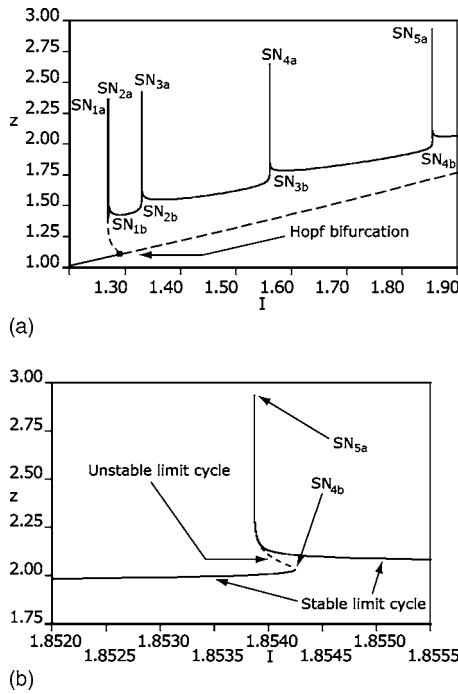


FIG. 4. Maximal z values associated with the stationary solutions of the complete HR model as a function of the external current I . In (a) the subcritical Hopf bifurcation where the FP loses its stability (filled circle) and the cascade of period-doubling saddle-bifurcations leading from bursts with one spike to bursts with five spikes. In (b) an enlargement of the bifurcation diagram in proximity of the transition from a burst with four-peaks to bursts with five-peaks is reported. Solid (resp. dashed) lines refer to stable (resp. unstable) solutions.

the new peak is located quite far from the rest of the packet of spikes and the period of the burst is peculiarly long, but for increasing currents the new peak rapidly reapproaches the old ones and the period of the whole burst returns at values similar to those preceding the SN_{4b} bifurcation [as displayed in Fig. 5(b)]. Please notice that this transition occurs in an extremely narrow current interval and it could be very difficult to clarify all these aspects without the help of a continuation software, like AUTO 2000.¹³

This sequence of period adding nonchaotic bifurcations repeats until the burst reaches 11 peaks as shown in Fig. 2(a), in particular the bursts emerging from these successive bifurcations are quite different from the one observed at lower currents [reported in Figs. 3(b) and 5]. Since now the solution never follows precisely the FP stable branch of the FS [as clearly shown in Fig. 6(a)] and this is probably due to the fact that the FP of the complete HR model is now located far from the stable branch of the FS. However, the arrangements of successive spikes within a burst is quite peculiar and it can be summarized as follows:

- Each successive spike has a decreasing height x_{peak} (i.e., the maximal x -value corresponding to each peak decreases).
- Each successive peak is associated with larger z -values (i.e., the position of the peak z_{peak} increases).
- The duration of each successive ISI within a burst, following the initial silent phase, is monotonically increasing.

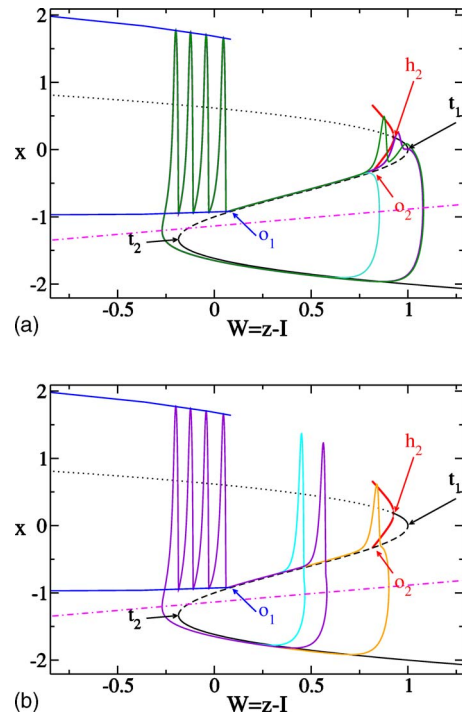


FIG. 5. (Color online) Curves and axis analogous to those displayed in Fig. 3. In (a) are reported the unstable bursts for three current values below the bifurcation SN_{5a} . The period of the solutions as well as the height of the extra peak increase by approaching SN_{5a} ; i.e., for decreasing currents. Namely, the three lines refer to $I=1.8541367086$, $I=1.8541367023$, and $I=I^*$. In (b) are reported a few stable solutions above the bifurcation SN_{5a} , the period of the solutions decreases for increasing current values $I^* < I \leq 1.854140$. The symbols are as in Fig. 1 and the dot-dashed z -nullcline refers to $I=I^*$.

All these facts can be appreciated in Figs. 6(a) and 6(b). The first two characteristics are due to the peculiar arrangement of the branch of periodic solutions P1 in the phase space shown in Fig. 1, while the third one can be explained by noticing that by moving along the burst the solution approaches the (unstable) FP. Therefore, the velocity of the orbit along each successive loop tends to decrease giving rise to longer and longer ISIs. A bursts with the above characteristics will be termed *regular*.

The structure of the bursts can be better appreciated by considering the ISI return map, displayed in Fig. 6(b). In this representation the silent regime is characterized by an extremely long ISI (a maximum in the map); the successive iteration of this point leads to an extremely low ISI, that corresponds to the period separating the 2 first spikes of the burst. The monotonic increase of the ISIs for the successive spikes is associated with points of the map lying on a line bending upwards with respect to the bisectrix [as it can be seen in the inset of Fig. 6(b)]. Moreover the ISI map is almost tangent to the diagonal for small ISI values, thus suggesting that the dynamics of the system could be interpreted as a intermittent behavior between a laminar phase characterized by regular spiking (a point on the diagonal would correspond to a tonic spiking regime) and a reinjection phase denoted by silence.⁶

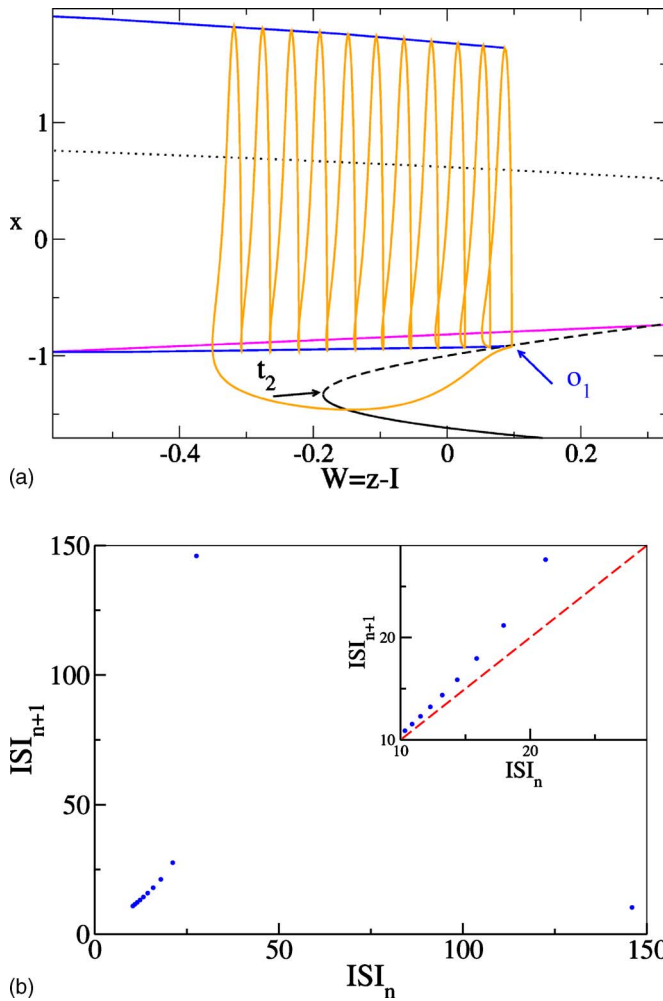


FIG. 6. (Color online) (a) Extrema of x corresponding to the stationary solutions of the FS vs W , together with a 11-peaks stable burst for $I=3.13$. The symbols are as in Fig. 1 and the solid (magenta) lines are the z null cline for the examined current. (b) The ISI return map for the same solution, in the inset an enlargement of the map together with the diagonal (red dashed line) is reported.

The successive bifurcation towards a burst with 12 peaks is more complicated, in particular it is chaotic, and it will be addressed in the next section.

V. THE CHAOTIC PHASES

In the following the chaotic regions of the model will be characterized in terms of a Lyapunov analysis and of the ISI return maps. In particular, we will mainly focus on the parameter value $r=0.0021$ (i.e., the value considered by González-Miranda in Ref. 7), however we will also discuss some aspect of the dynamics for $r=0.0010$ (i.e., the value examined by Wang in Ref. 6).

A. Lyapunov analysis

As a first step we have examined the degree of chaoticity of the model in terms of the associated Lyapunov spectrum for $r=0.0010$ and $r=0.0021$. In both cases one can observe chaotic regions characterized by a positive maximal Lyapunov exponent λ_1 .

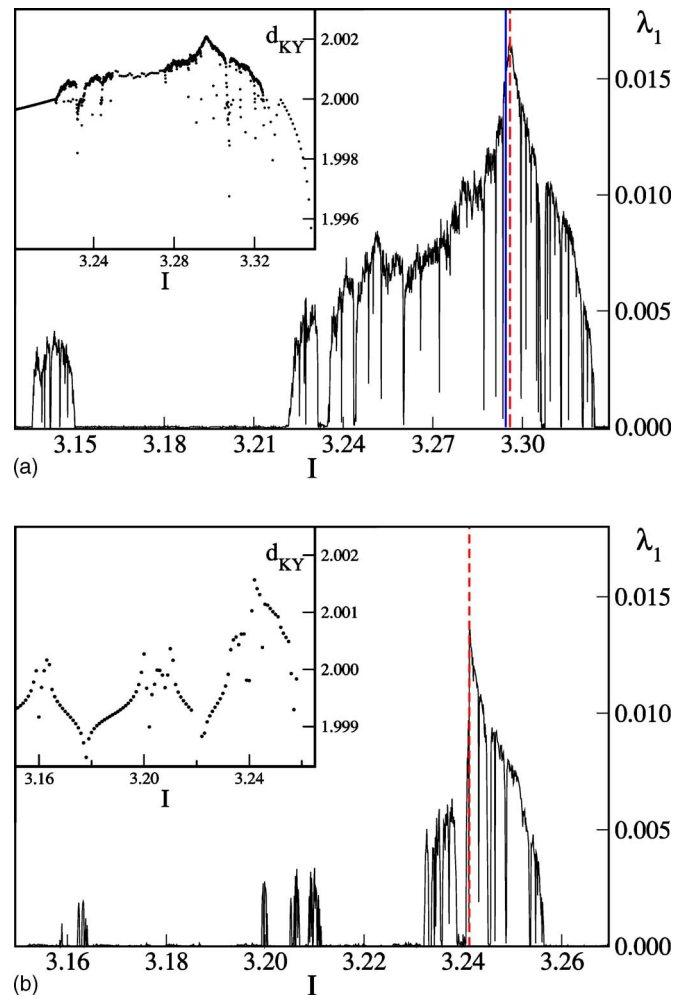


FIG. 7. (Color online) Maximal Lyapunov exponents λ_1 as a function of the external current I . (a) $r=0.0021$; (b) $r=0.0010$. The dashed lines represent I_G (resp. I_W) in (a) [resp. (b)], while the solid lines refer to the corresponding I_S . In the insets are reported the fractal dimensions d_{KY} . The data have been obtained by following the linearized evolution of the system over a total time $t=100\,000$, after that a transitory of duration of 1000 has been discarded.

As shown in Fig. 7, at low currents for $r=0.0010$ several narrow chaotic intervals are observed within the bursting region (for $r=0.0021$ only one of these is indeed discernible). These chaotic intervals are associated (as shown in the next subsection) with period-adding bifurcations. Moreover, in both cases a wider chaotic interval where λ_1 reaches its maximal value is present. Within this interval, the transition from a regime where the chaotic dynamics is dominated by bursts [termed bursting chaos (BC)] to a (chaotic) dynamical phase where the spiking dynamics is prevalent [termed spiking chaos (SC)] will take place. However, it should be noticed that these chaotic regions are interrupted by stable periodic windows containing solutions of different complexity. As already mentioned, a common aspect is that the maximal Lyapunov attains a sharp maximum $\lambda_1 \sim 0.0166$ (resp. $\lambda_1 \sim 0.0137$) within this interval at $I_{\max}=3.2958(1)$ [resp. $I_{\max}=3.2414(1)$] for $r=0.0021$ (resp. $r=0.001$). Remarkably, these values are, within the error bars, coincident with the values previously identified as the transition points from BC to SC (see Fig. 7). In particular in Ref. 6 for $r=0.0010$ the

value $I_w=3.241\ 320\ 53(5)$ has been reported, while in Ref. 7 for $r=0.0021$ the transition was located at $I_G=3.295\ 85$.

As far as the Kaplan-Yorke dimension is concerned we can observe (see the insets of Fig. 7) that its value is essentially 2 in the whole examined current intervals apart corrections of the order of 10^{-3} and that its behavior reflects that of λ_1 . Thus supporting the idea that a one-dimensional map could well reproduce the dynamics of the continuous system.

B. Period-adding chaotic bifurcation

Let us now consider for $r=0.0021$ the period-adding transition from a burst with 11-peaks to a burst with 12-peaks, as already mentioned this is characterized by chaos. The system is chaotic in the interval $[3.135\ 74; 3.1499]$, immediately before one has a stable 11-peak burst and immediately after a stable burst with 12-peaks is observable. However, the destabilization of the 11-peak burst is not trivial, because this burst bifurcates via period doubling at a current $I_{pd}=3.135\ 762(1)$ larger than the one associated with the onset of chaos. Therefore there is a small region of coexistence of chaotic and regular solutions. The main characteristic of this chaotic region is the appearance of *anomalous* burst, with this term we indicate bursts where successive ISIs within a burst are no more monotonically increasing (or correspondingly x_{peak} and z_{peak} are no more monotonic). This means that the spiking phase (within the burst) is no more characterized by a monotonous motion towards the homoclinic point o_1 followed by a slow silent (rejection) phase (SP), but that once the solution arrives in proximity of o_1 it can be reinjected (without any SP) at some intermediate point of the burst from where it restarts spiking. An example of an anomalous and a regular burst is reported in Fig. 8(a). These bursts will be denoted by the number of spikes N before the rapid reinjection and by the number of spikes M emitted in the following period before the SP separated by the letter a; e.g., $[12a2]$ indicates a burst of 12 peaks followed by two further peaks emitted after a rapid reinjection phase. In particular, we have observed only anomalous spikes with $M \geq 2$.

Typically, in the proximity of I_{pd} one observes a majority of regular bursts with 11 peaks (characterized by different duration in the SP), some regular burst with 12 peaks, and an increasing number of anomalous bursts with 13 or 14 peaks (typically of the type $[11a2]$ $[11a3]$). As shown in Fig. 8(b) by increasing I the number of regular or anomalous bursts containing 11 peaks rapidly declines while the density of bursts containing 12 peaks increases and reaches one at $I = 3.1500$, the chaotic interval is however interrupted by stable windows. In particular we have identified at $I = 3.1399$ a stable periodic solution composed of four bursts with different number of spikes: the solution can be identified by the number of spikes in each burst as $[12, 11, 11, 11a2]$. Furthermore, within the current interval $[3.1417; 3.1420]$ another stable structure made of two bursts $[12, 11a2]$ is observable, and finally a stable solution made of 3 bursts, namely $[12, 12, 11a2]$, has been found for $I \in [3.1450; 3.1451]$. To summarize, the solution containing only bursts with 11 peaks becomes unstable around I

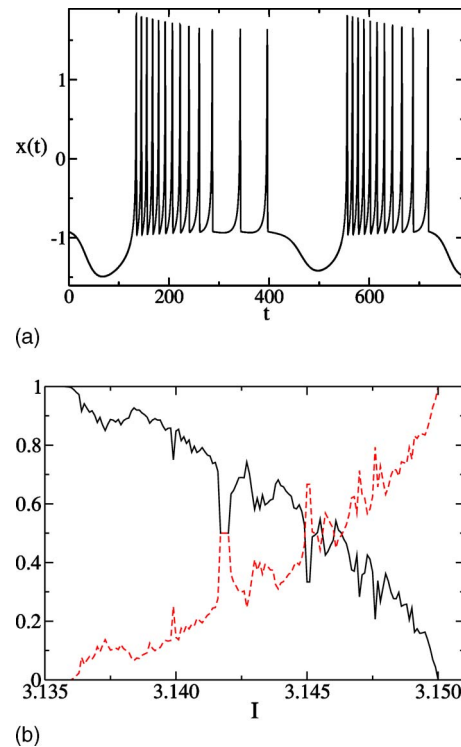


FIG. 8. (Color online) (a) The time evolution of the variable x for $I = 3.1360$ displaying one anomalous burst $[11a2]$ followed by a regular burst with 11 peaks. (b) Density of bursts (regular or anomalous) containing $N = 11$ (solid line) and $N = 12$ (dashed line) spikes. The density has been estimated over a statistics of 5000 bursts, after discarding a transient of 1×10^6 .

$= 3.1358$ and at the same time anomalous bursts (mainly of the type $[11a2]$ and $[11a3]$) begin to appear. By further increasing the current regular and anomalous bursts with 12 peaks appears and at $I = 3.1399$ a solution made of two regular bursts with 11 peaks, one burst with 12 peaks and an anomalous one $[11a2]$ get stabilized. At higher currents the bursts containing 12 peaks tend to prevail on the ones with 11 peaks and at the same time the number of anomalous bursts begins to decline and finally disappears [see Fig. 9(a)].

An interesting aspect of this transition is that the number of anomalous bursts is somehow related to the degree of chaoticity of the system. As shown in Fig. 9(a), the maximal Lyapunov is nonzero in the same region where anomalous bursts are present, moreover the density of anomalous bursts show a similar dependence on the current, apart in proximity of the stable windows containing bursts of the type $11a2$. The correlation between the density of anomalous bursts and λ_1 is not as simple as a proportionality, since as already mentioned also anomalous bursts can eventually become stable. In particular, it seems that the anomalous bursts with 12 peaks (that never get stabilized within the considered current interval) better correlate with λ_1 [see Fig. 9(a)].

Similar to what done in Ref. 17 for the Sherman's model, a useful characterization of this chaotic regime can be achieved in terms of the ISI return map.¹⁷ A typical example is shown in Fig. 9(b): the map is quite peculiar presenting a broad maximum with two horns. Each burst can be defined as a series of spikes separated by a "sufficiently long" ISI (the

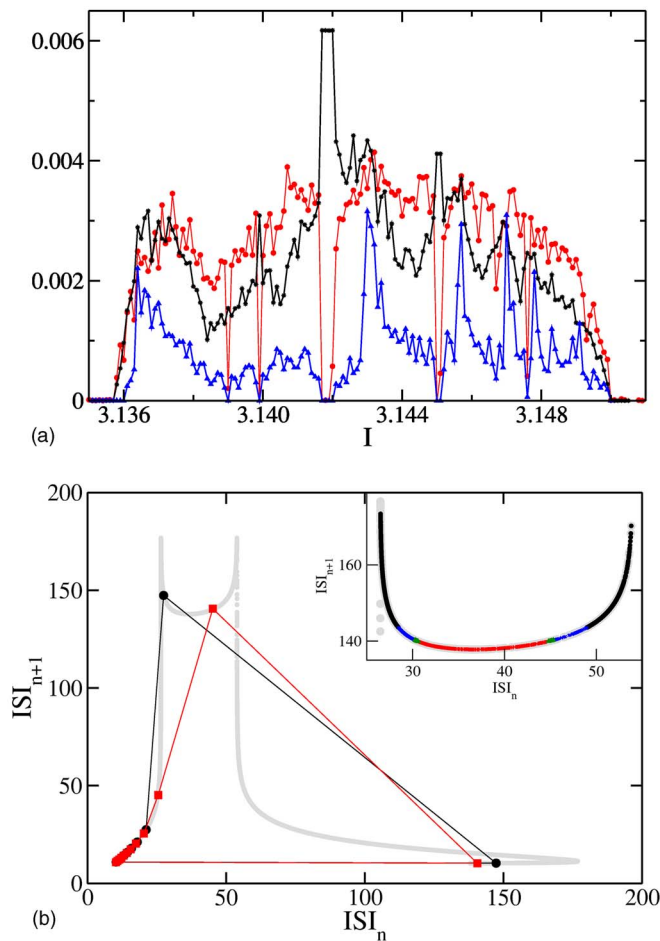


FIG. 9. (Color online) (a) Maximal Lyapunov exponent λ_1 (filled circles) vs the external current I . On the same graph are reported in arbitrary units the density of anomalous bursts (stars) together with the density of anomalous bursts of the type $12aM$ only (filled triangles), where M can be any number. The Lyapunov have been estimated, after a transient of duration 2×10^5 , by following the tangent dynamics for an analogous time, while the densities have been obtained by averaging over a statistics of 5000 bursts. (b) The ISI return map for chaotic solutions (gray dots) corresponds to $I=3.1407$, for stable bursts of period 11 (filled circles) to $I=3.1350$ and for stable bursts with 12 peaks (filled squares) to $I=3.1500$. The lines connecting the data have been maintained for the stable solutions as a guide for the eyes. In the inset is reported an enlargement of the upper part of the map showing the SPs. The gray dots refer to SPs of bursts of any kind, while SPs preceding [11] (filled circles), [11aM] (crosses), [12aM] (triangles), and [12] (plus) correspond to decreasing ISI values, respectively. The data have been taken after discarding transients of 10^6 – 10^7 .

SP), in particular we define a SP as an ISI longer than a certain threshold ISI_{th} (in the present case $ISI_{th}=135$). For these current values a burst is preceded and followed by a SP, therefore there is an ambiguity in identifying which SP should be associated with a certain burst. We noticed that the duration of the SP preceding the burst identifies in a unique manner the number of spikes and the type (anomalous or regular) of the following burst. Therefore it is natural to consider a burst as made by a reinjection phase followed by a spiking phase. In particular, with reference to the inset of Fig. 9(b), we observe that regular bursts with 11 peaks follow the longest SPs, while shorter SPs are associated with burst of the type [11aM] and [12aM]-bursts correspond to

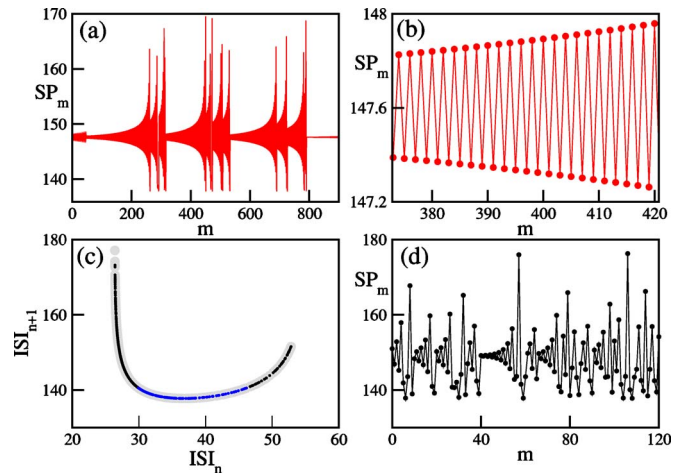


FIG. 10. (Color online) (a) Sequence of SPs as a function of the burst index m ; (b) enlargement of figure (a); (c) upper part of the ISI return map displaying SP (here indicated as ISI_{n+1}) as a function of the previous ISI; (d) sequence of SPs as a function of the burst index m . In (c) the SPs preceding a regular (anomalous) burst with 11 peaks are associated to higher (lower) values. Figures (a), (b), and (c) refer to $I=3.1359$ and (d) to $I=3.1407$.

even shorter SPs. Regular bursts with 12 peaks have SPs located at the bottom of the upper part of the map shown in the inset of Fig. 9(b).

The origin of the two horns in the ISI return map is related to the way the 11-peaks burst becomes unstable in the present case. In particular the dynamics in proximity of the chaotic onset is characterized by a sequence of bursts with “oscillating” value of SPs [as shown in Figs. 10(a) and 10(b) for $I=3.1359$]. In this case the SP-values oscillate around the value of the SP corresponding to the unstable burst with 11-peaks, moreover their distance with respect to the reference SP increases in time. This oscillating behavior is interrupted by abrupt collapses of the orbit to a neighborhood of the unstable periodic solution, followed again by oscillations of increasing amplitude. These oscillations are probably due to the fact that the unstable 11-peaks burst is a focus (i.e., it is characterized by complex Floquet exponents). This is at the origin of the two horns, since the SP (and also the ISI within the bursts) oscillates around an average value [see Fig. 10(c)]. Therefore by starting from almost identical initial conditions one can finish to one or to the other of the two horns of the ISI return map. This characteristic of the map is not only present in proximity of the bifurcation, but it is also a peculiarity of the BC for this model. As shown in Fig. 10(d) deep inside the chaotic interval, namely for $I=3.1407$, oscillations of successive SPs around the unstable 11 peaks structure are still present, but now the dynamics is more irregular due to the presence of bursts with different numbers of peaks.

C. The transition from bursting to spiking chaos

At higher currents the stable burst with 12 peaks becomes chaotic via a period-doubling cascade, taking place within the current interval [3.2210:3.2217]. Moreover, also in the chaotic phase the dynamics of the system remains often trapped in proximity of a burst with 12 peaks, as it can be clearly seen from Fig. 2(b) where the 12 peaks structure is

still discernible up to currents $I \sim 3.29\text{--}3.30$. Therefore, we can safely affirm that this elementary structure should be the most relevant to examine in order to understand the origin of the transition from bursting to spiking chaos.

Let us briefly describe the different dynamical regimes encountered by increasing the current I . As already mentioned, the 12-peaks burst follows a period doubling route to chaos. The 12-peaks solution remains stable up to $I = 3.2210$ then it bifurcates to a 24-peaks solution. This transition from a 12 to a 24-peaks burst is hysteretic, since the 24-peaks solution is stable in the range $[3.2205; 3.2214]$ that overlaps with the stability range of the 12-peaks solution. Furthermore, at $I \sim 3.2215$ the stable burst with 24 peaks bifurcates to a 48-peaks structure (that remains stable in the window $[3.2215; 3.2216]$) and this is then subjected to a rapid period doubling cascade finally leading to chaos for $I \geq 3.2217$ (this is also confirmed from the Lyapunov analysis).

Initially, in a narrow range of currents (namely $[3.2217; 3.2224]$) the only solutions giving rise to the chaotic dynamics are regular bursts with 12 peaks. In particular, the initial 12-peaks burst should have become an unstable focus, since the associated ISI return map reveals again the two horns structure previously discussed in Sec. V B. Around $I = 3.2225$ the system begins to display several different bursting solutions, namely regular and anomalous bursts with 12 peaks (the great majority) and shorter (regular and anomalous) bursts with 11–7 peaks. The corresponding ISI return map is still characterized by a broad maximum with 2 horns.

For higher I -values the system becomes more chaotic and reveals an increasing number of anomalous 12-peaks bursts (mainly of the type $[12a2]$ and $[12a3]$) together with anomalous and regular bursting solutions with a smaller number of peaks. The chaotic region is interrupted by several narrow stability windows, in particular we have identified the following ones: a first one at $I = 3.2253(1)$ characterized by the presence of an anomalous burst of the type $[12a3]$; a second one at $I = 3.2269(1)$, where a three bursts solution $[12, 12, 12a4]$ is encountered, and a third one at $I = 3.2274(1)$ in which a solution $[12, 12a2]$ is observed. At higher currents a wide nonchaotic interval appears for $I \in [3.2316; 3.2349]$, in this interval only solutions containing bursts of the type $[12a2]$ are observables. In particular, within this interval the elementary $[12a2]$ burst is subjected to a period doubling cascade leading to a chaotic dynamics where only $[12a2]$ bursts are represented (namely for $3.2350 \leq I \leq 3.2355$). Regular and anomalous 13-peaks burst solutions begin to manifest around current $I \sim 3.2403$, and a stable window characterized by bursts of the type $[13a2]$ is found for $3.2436 \leq I \leq 3.2442$, within this window a period-doubling cascade involving as elementary structure the burst $[13a2]$ is observed.

The dynamics in the range $I \in [3.245; 3.289]$ is essentially characterized by bursting solutions (regular or anomalous) with 13 or 12-peaks plus an increasing number of isolated spikes observables in between the bursting solutions. This observation can be made more quantitative by estimating the average number of spikes $\langle M \rangle$ emitted after a regular burst and before the successive SP (see Sec. V B).

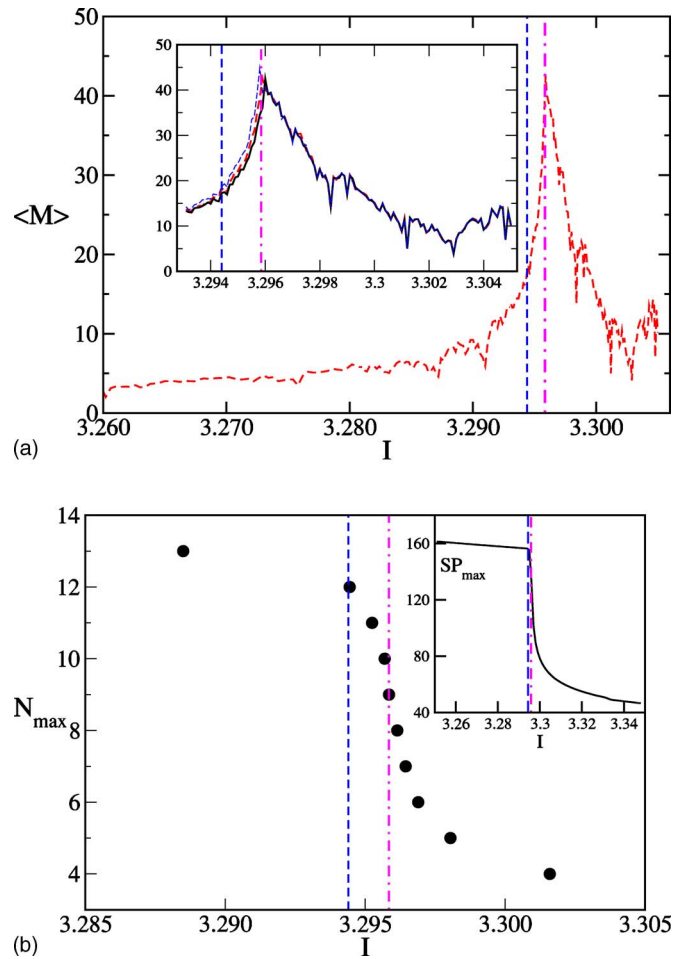


FIG. 11. (Color online) (a) Average number of spikes following a regular burst $\langle M \rangle$ as a function of the external current I . An enlargement is shown in the inset, where the three reported lines refer to different thresholds, employed for the identification of the SPs: namely, $SP_0 = 130$ (solid line); $SP_0 = 135$ (dashed line); $SP_0 = 140$ (dotted line). (b) Maximal number of spikes observed within a regular burst N_{\max} as a function of the current I , in the inset is reported SP_{\max} still vs I . The vertical dot-dashed line indicates the value of I_G , while the vertical dashed line refers to I_S . The data have been obtained after discarding a transient $t \sim 10^6$.

(The quantity M has been defined in Sec. V B and it can be evaluated by counting the number of spikes following a regular burst and preceding the successive SP.²⁴) This quantity is steadily increasing with I and reaches a maximal value around $I \sim 3.296$ [as shown in Fig. 11(a)]. The exact position of the maximum slightly depends on the employed value SP_0 . However, this maximum is located around $I \sim 3.2958\text{--}3.2960$ almost in correspondence of the current I_{\max} for which the system is maximally chaotic and of I_G previously identified in Ref. 7 as the transition point from BC to SC.

Above $I = 3.2885$ no (regular or anomalous) burst with 13-peaks is observable and the maximal number of bursts within a regular spike is again 12. For larger currents the dynamical behavior becomes more complicated, since now bursts can coexist with spikes and it is difficult to discriminate between the two kind of solutions. Since the 12-peak bursts seem to have a peculiar relevance in the dynamics of the model, we have decided to focus on bursts with the

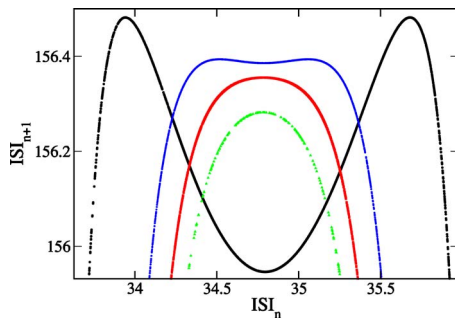


FIG. 12. (Color online) Upper part of the ISI return maps for various current values: (circles) $I=3.2934$; (asterisks) $I=3.2942$; (squares) $I=I_S=3.2944$, and (triangles) $I=3.2945$. The two horns are clearly visible for $I=3.2934$, while at $I=3.2942$ they are reduced to two shoulders, they merge at $I=I_S$ and only one hump remains at $I=3.2945$.

higher number of spikes, that in turn corresponds to the longer measured SPs. As shown in Fig. 11(b), the (regular) bursts with maximal number of spikes N_{\max} decreases rapidly for increasing I in correspondence with the drop of SP_{\max} . This drop has been previously identified as a signature of a *continuous interior crisis* leading from bursting to spiking chaos.⁷ From our analysis it emerges that this *continuous crisis* is related to a rapid disappearance of bursts with many peaks, in the region $3.290 \leq I \leq 3.301$ there is a sort of inverse cascade leading from bursts with at most 12 peaks to bursts with at most 3 peaks. Therefore the crisis is associated with the disappearance of long lasting bursting solutions. On the other hand, it should be stressed that isolated bursting solutions are clearly observable (even if immersed in trains of spikes) up to currents $I \sim 3.30$. This last observation indicates that the crisis indeed leads from a dynamics dominated by bursts to one dominated by spikes, but both solutions coexist above and below the transition.

We have also noticed that the beginning of the transition (from the bursting side) is associated with a structural modification of the ISI return map. As shown in Fig. 12, the ISI return map is characterized by two horns up to $I_S = 3.2944(1)$, while for higher currents the two horns merge giving rise to a map with a single hump. It should be noticed that exactly at $I=I_S$ the bursts with 12-peaks disappear, while the destabilization of this kind of orbits was at the origin of the onset of the BC. The two horns in the map have been previously associated with an “oscillatory” divergence from some bursting solution (representing an unstable focus). The structural modification of the map and the contemporary disappearance of 12-peaks solutions indicates that the peculiar dynamics was intimately related to this kind of bursting orbits. A similar analysis performed for $r=0.001$ (i.e., the value studied in Ref. 6) confirms the previous results, giving the following critical value for the structural transition $I_S = 3.241\,320\,040(5)$, that is not too far from the value reported by Wang, i.e., $I_W = 3.241\,320\,53(1)$. Moreover, the structural transition is again associated with the disappearance of the family of (anomalous or regular) bursts containing 23 peaks, and once more these solutions are the most relevant for the chaotic bursting dynamics at this r -value.

As we have already mentioned, the previously published analysis of the “bursting-spiking” transition suggested that it

should be a sort of (interior) crisis that destabilizes the chaotic phase of continuous spiking and leads to a state characterized by chaotic bursting.^{6,7} However, as we have shown bursting solutions can be found for $r=0.0021$ up to currents $I \sim 3.30$, currents that are deeply inside the region of spiking chaos, accordingly to the criteria of González-Miranda, who found $I_G = 3.295\,85$ as the transition value, and Wang, that, as we have numerically verified, gives a similar value $I_W = 3.295\,88(1)$.

While González-Miranda⁷ has identified the transition as a sharp drop in the size of the three-dimensional attractor (or equivalently in the SP_{\max} value), Wang⁶ claimed that the 2D invariant manifold associated with the stable and weakly unstable directions of the unstable FP should play a fundamental role in the origin of the bursting behavior. In particular, Wang has suggested that an orbit approaching the FP would remain in the oscillatory region or escape towards the bursting attractor, depending on which side of the 2D manifold it would fall. In other words, since each orbit (within the transition region) evolves in time towards the FP, the reinjection mechanism would lead the orbit towards the bursting or spiking solutions depending if the trajectory would (in proximity of the FP) fall on one side or on the other of the 2D invariant manifold. However, due to the difficulties in evaluating the nonlinear manifolds, Wang was obliged to adopt several approximations to verify the validity of his transition criterion. In particular, he considered the linearization of the invariant manifolds and, in order to examine the trajectories in proximity of the FP, he has taken a Poincaré section located at a small (arbitrary) distance from the FP itself. Unfortunately, the points lying on this Poincaré map are not only the points in the reinjection region, but points located all along the trajectory. In particular, as we have verified, the points responsible for the validation of the “transition criterion” are the more distant from the FP (the ones with the smaller z -values). From our analysis we can conclude that the Wang’s criterion is essentially able to capture a strong increase in the size of the attractor (along the z direction). This would explain why the value estimated by us (employing Wang’s criterion) almost coincide with the I_G value. To conclude we cannot affirm that the mechanism responsible for the occurrence of bursting solutions suggested by Wang is wrong, but the implementation of the exact criterion is extremely difficult and the approximated test reported in Ref. 6 seems to be quite questionable.

VI. SUMMARY

A detailed analysis of the dynamical regimes of the Hindmarsh-Rose model has been here reported. In particular, we focused on the characterization of dynamical phases presenting bursting solutions. These emerge from the resting state via a cascade of period-adding bifurcations. All these bifurcations present similar features: the stable burst with n -spikes disappears (via a saddle-node bifurcation) by colliding with an unstable branch that continuously connects this solution to the stable $n+1$ -spikes burst emerging in correspondence of a tangent bifurcation at a lower current value. During the bifurcation the period of the burst becomes ex-

tremely long, similar to what was predicted by Terman for continuous period-adding bifurcations.⁸ At variance with the results of Terman the period increase occurs along a branch of unstable solutions and the increase is due to the fact that the period-adding is realized by connecting two distinct families of periodic solutions exhibited by the fast subsystem.

Also chaotic period-adding bifurcations have been observed for this model, and the origin of the chaotic dynamics can be ascribed to the occurrence of *anomalous* bursts. These bursts do not present, as the *regular* ones, a monotonic increase of the ISI periods following the initial silent (rest) period. In particular, the density of the anomalous bursts appear to be correlated with the level of chaoticity of the system.

As already pointed out in two previous works,^{6,7} the transition from bursting to spiking chaos resembles a crisis, since it is associated with an abrupt (but continuous) reduction of the size of the chaotic attractor. We have shown that this kind of crisis is associated with a sharp peak in the maximal Lyapunov exponent and in the average number of spikes not belonging to regular bursts. Therefore, once more the chaotic activity in the system (on the bursting side) seems to be related to the occurrence of *irregular* spikes in between *regular* bursts. It should be noticed that bursting and spiking solutions coexist over the whole range of the transition making a clear distinction of the two phases quite difficult. However, the maximal number N_{\max} of peaks observable, for a certain current, within a single *regular* burst can be employed as an order parameter to characterize the transition itself. A vanishing of N_{\max} will clearly indicate that we are in a phase characterized only by spiking solutions. Indeed N_{\max} has a sharp drop in correspondence of the attractor size shrinking. Furthermore, the beginning of the transition (from the bursting side) is marked from a structural modification of the ISI return map together with the disappearance of the family of bursts responsible for the onset of the bursting chaos.

These characteristics resemble another chaos-chaos transition: the phase to defect-turbulence transition observed for the complex Ginzburg-Landau equation (CGLE).²⁰ Also in that case the transition from one dynamical regime to another was related to the disappearance of a family of unstable solutions of the CGLE.²¹ However, at variance with the present situation no indication of the transition was possible to infer from the Lyapunov analysis.²²

The analysis reported here can be of interest not only among the scientists working on nonlinear dynamical systems, but also for the neuroscience community. We believe that the characterization we have performed for the Hindmarsh-Rose model can be useful in clarifying similar transitions observed for other models of bursting neurons¹¹ and hopefully can be of some utility for a better comprehension of neuronal information transmission. In particular, as recently suggested in Ref. 11 an efficient and robust coding

of the dynamics can be achieved in neuronal models presenting a cascade of period adding bifurcations, by introducing different universality classes, each one labeled by the period of the bursting solution dominating such dynamical phase.

ACKNOWLEDGMENTS

We thank G. Giacomelli and L. Citi for their collaboration in the initial stages of this study. Useful discussions with J.-M. Ginoux, R. Lima, and M. Lefranc during the *Journées de Dynamique Non Linéaire* that took place in Marseille, France in November 2006, are warmly acknowledged, as well as clarifications and hints received by S. Yanchuk and S. Lepri. J. Rubin is acknowledged for his critical reading of the unpublished manuscript. This work has been partially supported by the Italian Ministry of University and Research (MIUR), under the Project PRIN 2005 No. 2005098133-003 “Nonlinear dynamic networks: techniques for robust analysis of deterministic and stochastic models.”

¹J. L. Hindmarsh and R. M. Rose, Proc. R. Soc. London, Ser. B **221**, 87 (1984).

²T. R. Chay, Biol. Cybern. **52**, 339 (1985); Physica D **16**, 233 (1985).

³T. R. Chay and J. Kaizer, Biophys. J. **42**, 181 (1983).

⁴T. R. Chay and J. Rinzel, Biophys. J. **47**, 357 (1985).

⁵A. Sherman, J. Rinzel, and J. Kaizer, Biophys. J. **54**, 411 (1988).

⁶X. J. Wang, Physica D **62**, 263 (1993).

⁷J. M. González-Miranda, Chaos **13**, 845 (2003).

⁸D. Terman, SIAM J. Appl. Math. **51**, 1418 (1991).

⁹Z. Q. Yang and Q. S. Lu, Chin. Phys. Lett. **21**, 2124 (2004).

¹⁰E. Mosekilde, B. Lading, S. Yanchuk, and Y. Maistrenko, BioSystems **63**, 3 (2001).

¹¹J. M. González-Miranda, Phys. Rev. E **72**, 051922 (2005).

¹²D. Terman, J. Nonlinear Sci. **2**, 135 (1992).

¹³E. J. Doedel, R. C. Paffenroth, A. R. Champneys, T. F. Fairgrieve, Yu. A. Kuznetsov, B. Sandstede, and X. Wang, “AUTO 2000: Continuation and bifurcation software for ordinary differential equations (with HomCont),” Technical Report, Caltech (2001).

¹⁴I. Shimada and T. Nagashima, Prog. Theor. Phys. **61**, 1605 (1979); G. Benettin, L. Galgani, A. Giorgilli, and J-M Strelcyn, Meccanica **15**, 21 (1980).

¹⁵J. L. Kaplan and J. A. Yorke, Lect. Notes Math. **13**, 730 (1979).

¹⁶A. V. Holden and Y. Fan, Chaos, Solitons Fractals **2**, 221 (1992); **2**, 349 (1992); **2**, 583 (1992).

¹⁷J. Aguirre, E. Mosekilde, and M. A. F. Sanjuán, Phys. Rev. E **69**, 041910 (2004).

¹⁸T. Sauer, Phys. Rev. Lett. **72**, 3811 (1994).

¹⁹J. C. Alexander and D.-Y. Cai, J. Math. Biol. **29**, 405 (1991).

²⁰I. S. Aranson and L. Kramer, Rev. Mod. Phys. **74**, 99 (2002).

²¹L. Brusch, M. G. Zimmermann, M. van Hecke, M. Bär, and A. Torcini, Phys. Rev. Lett. **85**, 86 (2000).

²²D. A. Egolf and H. S. Greenside, Nature (London) **369**, 129 (1994).

²³A cascade of chaotic period adding bifurcations, characterized by saddle-node chaos-periodicity transitions, has been recently observed for the HR model by varying the internal control parameter r , Ref. 11.

²⁴However, this definition is meaningful only if one is able to define unambiguously the SPs. This is true if there is almost a gap in the ISI-distribution between regular ISIs and the SPs, otherwise the discrimination can be more difficult. In practice, we have identified a generic ISI as a SP if its duration is longer than a certain threshold SP_{th} . The threshold has been initially fixed to a constant value SP_0 (typically, $SP_0=135$) if the maximal SP (i.e., SP_{\max}) is larger than SP_0 , otherwise we fixed $SP_{th}=SP_{\max}-5$. As shown in Ref. 7, SP_{\max} at low currents $3.25 \leq I \leq 3.294$ is always of the order 150–160 and there is almost a gap in the ISI distributions that allows for a meaningful definition of the SP with any threshold in the range $150 \leq S_0 \leq 100$; see also the inset of Fig. 11(b).